

# Fine-Grained Representation Learning via Multi-Level Contrastive Learning without Class Priors

Houwang Jiang<sup>a</sup>, Zhuxian Liu<sup>a</sup>, Guodong Liu<sup>a</sup>, Xiaolong Liu<sup>a</sup>, Shihua Zhan<sup>a,\*</sup>

<sup>a</sup>*School of computer science and information engineering, Fujian Agriculture and Forestry University, Fuzhou, 350002, China*

---

## Abstract

Recent advances in unsupervised representation learning frequently leverage class information to improve the extraction and clustering of features. However, this dependence on class priors limits the applicability of such methods in real-world scenarios where class information is unavailable or ambiguous. In this paper, we propose *Contrastive Disentangling (CD)*, a simple yet effective framework that learns representations without any relying on class priors. CD employs a multi-level contrastive learning strategy, integrating instance-level and feature-level losses with a normalized entropy loss to learn semantically rich and fine-grained representations. Specifically, (1) the instance-level contrastive loss encourages the separation of feature representations between different samples; (2) the feature-level contrastive loss promotes independence among feature prediction heads; and (3) the normalized entropy loss ensures that the feature heads capture meaningful and prevalent attributes from the data. These components together enable CD to outperform existing methods in scenarios lacking class priors, as demonstrated by extensive experiments on benchmark datasets including CIFAR-10, CIFAR-100, STL-10, and ImageNet-10. The code is available at <https://github.com/Hoper-J/Contrastive-Disentangling>.

**Keywords:** Disentangled representations, Clustering, Contrastive learning, Representation learning, Unsupervised learning

---

## 1. Introduction

The growing availability of large-scale unlabeled datasets has underscored the importance of unsupervised learning in extracting meaningful features without predefined class labels. In computer vision, contrastive learning has become a dominant method for unsupervised representation learning, improving feature extraction by maximizing consistency between augmented views of the same instance while minimizing similarity between distinct instances [1, 2].

Recent contrastive learning methods [3, 4, 5] have incorporated class priors to enhance performance. By using class counts as prior knowledge during network construction, these approaches achieve state-of-the-art results in unsupervised clustering tasks, indicating that class information can lead to more discriminative feature representations. However, this reliance on class priors limits their applicability in real-world scenarios where class information is uncertain.

To address this limitation, we propose Contrastive Disentangling (CD), a novel framework that refines feature extraction and disentanglement in unsupervised learning without relying on class priors. CD integrates multi-level contrastive learning with a disentanglement loss to ensure feature diversity and independence, making it applicable to scenarios lacking class information. Our approach avoids complex additional modules such as pseudo-labeling, focusing instead on the effectiveness of the core framework.

As shown in Figure 1, CD utilizes two levels of contrastive learning: instance-level and feature-level. Instance-level contrastive learning distinguishes image instances in the feature space, while feature-level contrastive learning

---

\*Corresponding author.

Email addresses: [hoper.hw@gmail.com](mailto:hoper.hw@gmail.com) (Houwang Jiang), [zhanshihua2004@fafu.edu.cn](mailto:zhanshihua2004@fafu.edu.cn) (Shihua Zhan)

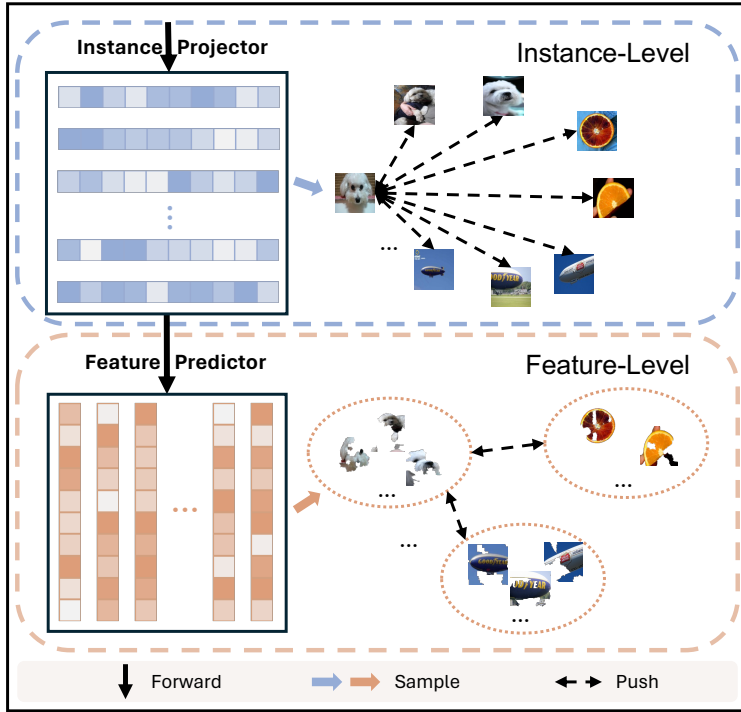


Figure 1: **Overview of the Multi-level Contrastive Learning Strategy in CD Framework.** The instance-level (top) operates on image instances, while the feature-level (bottom) focuses on features visualized using LIME.

ensures that distinct prediction heads capture diverse and complementary feature attributes. The feature-level module employs the LIME (Local Interpretable Model-Agnostic Explanations) technique [6] to visualize feature predictions, offering an intuitive interpretation of the model’s behavior. In summary, the main contributions of this paper are:

1. **Feature Prediction Heads:** We introduce feature prediction heads as a novel component in the feature learning process. Through the use of a normalized entropy loss, these heads effectively capture common features prevalent in the dataset, enhancing the representational capacity and generalization of the learned features.
2. **Feature-Level Contrastive Learning:** We propose a feature-level contrastive learning strategy to encourage different feature prediction heads to focus on distinct and complementary features, promoting effective feature disentanglement.
3. **Simple and Effective Framework:** We present a straightforward and effective framework that improves fine-grained feature learning in unsupervised tasks without relying on class priors. Extensive experiments on benchmark datasets demonstrate the superiority of CD, particularly in NMI scores. Ablation studies confirm the effectiveness of each component, providing new insights into unsupervised representation learning.

## 2. Related Work

### 2.1. Unsupervised Representation Learning

Unsupervised representation learning seeks to extract meaningful features from unlabeled data. This area is dominated by two main approaches: generative models and contrastive learning. Generative models [7, 8, 9] aim to generate samples that resemble the true data distribution by modeling the underlying latent space. Despite their success in data generation, these models often struggle to learn invariant feature representations—features that remain consistent under various input transformations such as rotation, translation, and scaling [10].

To overcome these limitations, instance-level contrastive learning methods [2, 11, 12, 13] have been developed. These approaches enhance the model’s ability to extract invariant features by maximizing the similarity between different augmented views of the same instance while minimizing the similarity between different instances. As a result,

contrastive learning has proven to be highly effective across various downstream tasks, offering robust performance in unsupervised learning.

## 2.2. Utilization of Class Priors

Several recent approaches [4, 5, 14] have incorporated class prior information to improve model performance by constraining the final outputs based on known class counts. These methods often achieve state-of-the-art results in unsupervised clustering tasks by guiding the model to learn more discriminative feature representations. Additionally, pseudo-labeling techniques are sometimes employed to iteratively refine cluster assignments, further boosting performance.

However, these methods are limited by their reliance on class priors, making them unsuitable for real-world tasks where class labels are often unknown or ambiguous. This reliance highlights the need for methods that can operate effectively without class information.

## 2.3. Multi-level Contrastive Learning

Multi-level contrastive learning has emerged as a promising direction within contrastive learning research. The introduction of cluster-level contrastive learning by Li et al. [4] for clustering tasks has opened new avenues for exploring more structured representations. However, methods that partition data based on predefined categories may miss the fine-grained features inherent in more complex datasets, limiting their ability to capture nuanced representations.

Building on this insight, we propose the Contrastive Disentangling (CD) framework, which leverages feature space representations as inputs to multiple feature prediction heads. By combining feature-level and instance-level contrastive learning, CD encourages a decoupling of distinct feature heads, enabling the model to learn more diverse and fine-grained feature representations. This approach advances unsupervised representation learning without relying on class priors, offering a more flexible and robust solution for a variety of tasks.

## 3. Method

### 3.1. Proposed Contrastive Disentangling Framework

The proposed Contrastive Disentangling (CD) framework leverages a multi-level contrastive learning strategy to achieve fine-grained representation learning without the need for class priors, as illustrated in Figure 2. The CD framework comprises the following key components:

- **Data Augmentation:** Each input batch  $\mathbf{x}$  undergoes a series of data augmentation operations, including random cropping, horizontal flipping, color jittering, and Gaussian blurring. These augmentations generate two correlated views, denoted as  $\mathbf{x}^{(1)}$  and  $\mathbf{x}^{(2)}$ , of the same sample. This dual-view approach encourages the model to focus on semantically relevant features that are invariant to such transformations.
- **Feature Extraction:** The augmented views are processed by a shared backbone network  $f(\cdot)$ , implemented using a ResNet architecture [15]. This backbone extracts feature representations  $\mathbf{h}^{(1)} = f(\mathbf{x}^{(1)})$  and  $\mathbf{h}^{(2)} = f(\mathbf{x}^{(2)})$ , ensuring consistent feature extraction across different views.
- **Instance Projector:** The extracted features are passed through an instance projector  $g(\cdot)$ , a multi-layer perceptron (MLP) consisting of two linear layers with batch normalization [16] and ReLU activation functions. This projector maps the features into a latent space, producing latent representations  $\mathbf{z}^{(1)} = g(\mathbf{h}^{(1)})$  and  $\mathbf{z}^{(2)} = g(\mathbf{h}^{(2)})$ . These representations are then used for instance-level contrastive learning.
- **Feature Predictor:** To capture diverse and disentangled feature attributes, the latent representations are further processed by a feature predictor  $h(\cdot)$ . This module, structurally similar to the instance projector but with a sigmoid activation in the final layer, outputs predictions  $\mathbf{y}^{(1)} = h(\mathbf{z}^{(1)})$  and  $\mathbf{y}^{(2)} = h(\mathbf{z}^{(2)})$ . Each  $\mathbf{y}^{(v)}$  is a matrix of size  $N \times K$ , where  $K$  denotes the number of feature heads. Each feature head is designed to capture a distinct attribute of the data.
- **Loss Functions:** The total loss function of CD integrates three components: the instance-level contrastive loss  $\mathcal{L}_{\text{inst}}$ , the feature-level contrastive loss  $\mathcal{L}_{\text{feat}}$ , and the normalized entropy loss  $\mathcal{L}_{\text{entropy}}$ . These losses work synergistically to promote feature diversity, encourage independence among the learned features, and prevent feature collapse.

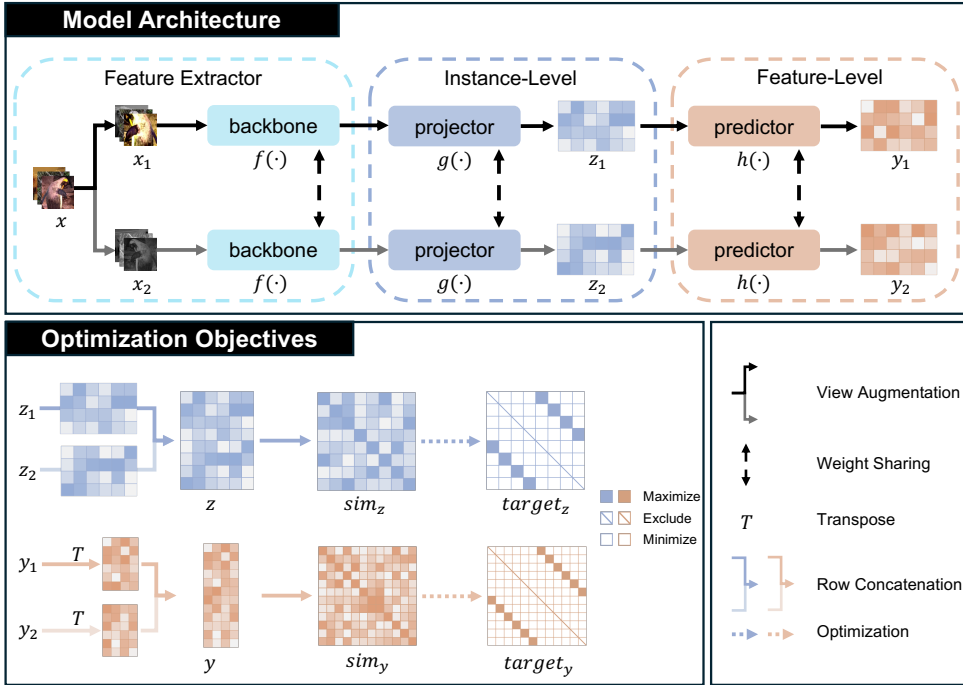


Figure 2: **Architecture of the proposed Contrastive Disentangling (CD) framework.** The upper section illustrates the shared backbone network, instance-level projector, and feature predictor, while the lower section displays the optimization objectives for instance-level and feature-level contrastive learning.

### 3.2. Instance-level Contrastive Learning

Instance-level contrastive learning aims to learn discriminative features by bringing representations of different augmented views of the same instance closer while pushing apart representations of different instances. This dual objective enhances the model’s ability to distinguish between distinct instances and recognize invariant features across different augmentations.

Given an input batch  $\mathbf{x}$  of size  $N$ , two augmented views  $\mathbf{x}^{(1)}$  and  $\mathbf{x}^{(2)}$  are generated. After passing through the backbone network and instance projector, latent representations  $\mathbf{z}^{(1)}$  and  $\mathbf{z}^{(2)}$  are obtained. These representations are concatenated to form a combined set of  $2N$  latent vectors:

$$\mathbf{z} = \begin{bmatrix} \mathbf{z}^{(1)} \\ \mathbf{z}^{(2)} \end{bmatrix} = \begin{bmatrix} \mathbf{z}_1 \\ \mathbf{z}_2 \\ \vdots \\ \mathbf{z}_{2N} \end{bmatrix} \in \mathbb{R}^{2N \times d}, \quad (1)$$

where  $d$  is the dimensionality of the latent space.

The similarity between any two latent representations is measured using cosine similarity:

$$\text{sim}_z(i, j) = \frac{\mathbf{z}_i \cdot \mathbf{z}_j}{\|\mathbf{z}_i\| \|\mathbf{z}_j\|} \quad (2)$$

for  $i, j \in \{1, 2, \dots, 2N\}$ . The purpose of using cosine similarity is to measure how closely related two feature vectors are, with a higher value indicating greater similarity. Building on this similarity measure, we define the instance-level contrastive loss  $\mathcal{L}_{\text{inst}}$ , which aims to maximize the similarity between positive pairs (i.e., the other augmented view of the same instance) and minimize the similarity between negative pairs (i.e., views of different instances). For each sample  $i$ , the instance-level contrastive loss is formulated as:

$$\ell_i^{\text{inst}} = -\log \frac{\exp(\text{sim}_z(i, \text{pos}(i)) / \tau_{\text{inst}})}{\sum_{k=1}^{2N} \mathbb{1}_{[k \neq i]} \exp(\text{sim}_z(i, k) / \tau_{\text{inst}})} \quad (3)$$

where  $\text{pos}(i)$  denotes the index of the positive sample corresponding to  $i$ ,  $\tau_{\text{inst}}$  is a temperature parameter controlling the concentration level of the distribution, and  $\mathbb{1}_{[k \neq i]}$  is an indicator function that equals 1 when  $k \neq i$  and 0 otherwise. This formulation follows the NT-Xent loss used in previous work [2, 17, 18, 19]. The total instance-level contrastive loss is computed by averaging over all  $2N$  samples:

$$\mathcal{L}_{\text{inst}} = \frac{1}{2N} \sum_{i=1}^{2N} \ell_i^{\text{inst}} \quad (4)$$

### 3.3. Disentanglement Loss

To ensure that the learned feature representations are both diverse and independent, we introduce two complementary loss functions: the feature-level contrastive loss, which promotes diversity by encouraging each feature head to focus on distinct attributes, and the normalized entropy loss, which ensures that the captured features are meaningful and prevalent across the dataset.

#### 3.3.1. Feature-Level Contrastive Loss

The feature predictor  $h(\cdot)$  produces predictions  $\mathbf{y}^{(1)}$  and  $\mathbf{y}^{(2)}$ , each of size  $N \times K$ , where  $K$  is the number of feature heads. To apply feature-level contrastive learning, we concatenate the transposed outputs of the two views:

$$\mathbf{y} = \begin{bmatrix} (\mathbf{y}^{(1)})^\top \\ (\mathbf{y}^{(2)})^\top \end{bmatrix} = \begin{bmatrix} \mathbf{y}_1 \\ \mathbf{y}_2 \\ \vdots \\ \mathbf{y}_{2K} \end{bmatrix} \in \mathbb{R}^{2K \times N}, \quad (5)$$

where  $\mathbf{y}_i$  represents the predictions of feature head  $i$  across the batch. The cosine similarity between any two feature prediction vectors is defined as:

$$\text{sim}_y(i, j) = \frac{\mathbf{y}_i \cdot \mathbf{y}_j}{\|\mathbf{y}_i\| \|\mathbf{y}_j\|} \quad (6)$$

The feature-level contrastive loss encourages each feature head to capture distinct attributes by maximizing the similarity between corresponding heads across different views while minimizing the similarity between different heads. For feature head  $i$ , the loss is defined as:

$$\ell_i^{\text{feat}} = -\log \frac{\exp(\text{sim}_y(i, \text{pos}(i)) / \tau_{\text{feat}})}{\sum_{k=1}^{2K} \mathbb{1}_{[k \neq i]} \exp(\text{sim}_y(i, k) / \tau_{\text{feat}})} \quad (7)$$

where  $\text{pos}(i)$  denotes the index of the positive sample for feature head  $i$ , and  $\tau_{\text{feat}}$  is the temperature parameter for the feature-level contrastive loss. The total feature-level contrastive loss is computed by averaging over all  $2K$  feature heads:

$$\mathcal{L}_{\text{feat}} = \frac{1}{2K} \sum_{i=1}^{2K} \ell_i^{\text{feat}} \quad (8)$$

#### 3.3.2. Normalized Entropy Loss

To prevent feature collapse and ensure that the learned features are meaningful and widespread across the dataset, we introduce a normalized entropy loss  $\mathcal{L}_{\text{entropy}}$ . This loss encourages each feature head to distribute its predictions evenly, capturing non-trivial and prevalent patterns in the data. The normalized binary entropy for each feature prediction vector  $\mathbf{y}_i$  is defined as:

$$H(\mathbf{y}_i) = -\frac{1}{N \log(2)} \sum_{j=1}^N (\mathbf{y}_{ij} \log(\mathbf{y}_{ij}) + (1 - \mathbf{y}_{ij}) \log(1 - \mathbf{y}_{ij})) \quad (9)$$

The overall normalized entropy loss is the average entropy across all feature heads:

$$\mathcal{L}_{\text{entropy}} = \frac{1}{2K} \sum_{i=1}^{2K} H(\mathbf{y}_i) \quad (10)$$

### 3.3.3. Combined Disentanglement Loss

The total disentanglement loss is the combination of the feature-level contrastive loss and the normalized entropy loss:

$$\mathcal{L}_{\text{disentanglement}} = \mathcal{L}_{\text{feat}} - \alpha \mathcal{L}_{\text{entropy}} \quad (11)$$

where  $\alpha$  is a hyperparameter that controls the balance between encouraging diversity and ensuring meaningful feature representations. By jointly optimizing these two objectives, the feature heads are encouraged to capture both diverse and informative patterns, leading to higher-quality feature disentanglement.

### 3.4. Total Loss

The total loss function for training the CD framework is the sum of the instance-level contrastive loss and the disentanglement loss. This ensures that both the instance-level discrimination and feature-level disentanglement are optimized simultaneously:

$$\mathcal{L}_{\text{total}} = \mathcal{L}_{\text{inst}} + \mathcal{L}_{\text{disentanglement}}. \quad (12)$$

By optimizing both the instance and feature-level objectives, our framework achieves a robust balance between learning discriminative instance-level representations and promoting diverse, meaningful feature representations without relying on class priors. Algorithm 1 summarizes the proposed method.

---

#### Algorithm 1: Contrastive Disentangling Framework

---

**Input:** Dataset  $X$ , Batch size  $N$ , Feature number  $K$ , Temperature constants  $\tau_{\text{inst}}$  and  $\tau_{\text{feat}}$   
**Output:** Total loss  $\mathcal{L}_{\text{total}}$

```

for each minibatch  $\mathbf{x}$  of size  $N$  in  $X$  do
    // Apply data augmentation
     $\mathbf{x} \rightarrow \{\mathbf{x}^{(1)}, \mathbf{x}^{(2)}\}$ ;
    for each view  $\mathbf{x}^{(v)}$ ,  $v \in \{1, 2\}$  do
        // Extract features
         $\mathbf{h}^{(v)} = f(\mathbf{x}^{(v)})$ ;
        // Project to latent space
         $\mathbf{z}^{(v)} = g(\mathbf{h}^{(v)})$ ;
        // Generate feature head predictions
         $\mathbf{y}^{(v)} = h(\mathbf{z}^{(v)})$ ;
    end
    Combine  $\mathbf{z}^{(1)}, \mathbf{z}^{(2)}$  by Eq.(1) and  $\mathbf{y}^{(1)}, \mathbf{y}^{(2)}$  by Eq.(5)
    // Compute Losses
    Compute cosine similarities  $\text{sim}_z(i, j)$ ,  $\text{sim}_y(i, j)$  by Eq. (2), (6);
    Compute instance-level contrastive loss  $\mathcal{L}_{\text{inst}}$  by Eq. (3), (4);
    Compute feature-level contrastive loss  $\mathcal{L}_{\text{feat}}$  by Eq. (7), (8);
    Compute normalized entropy loss  $\mathcal{L}_{\text{entropy}}$  by Eq. (9), (10);
    Compute total loss  $\mathcal{L}_{\text{total}}$  by Eq. (12);
    // Update Model Parameters
    Update  $f$ ,  $g$ , and  $h$  by minimizing  $\mathcal{L}_{\text{total}}$ ;
end
return  $\mathcal{L}_{\text{total}}$ 

```

---

## 4. Experiment

### 4.1. Datasets

We conducted experiments on four widely-used datasets: CIFAR-10, CIFAR-100 [20], STL-10 [21], and ImageNet-10 [22]. These datasets serve as benchmarks to rigorously evaluate the effectiveness of our proposed Contrastive

Table 1: Overview of datasets used for training and evaluation

Dataset	Split	Samples	Classes
CIFAR-10	train+test	60,000	10
CIFAR-100-20	train+test	60,000	20
STL-10	train+test	13,000	10
ImageNet-10	train	13,000	10

Disentangling (CD) framework. Table 1 provides an overview of the dataset splits, sample sizes, and the number of classes.

For CIFAR-100, we used 20 super-classes as ground-truth labels instead of the 100 fine-grained classes, aligning with benchmark settings in previous studies. Additionally, to guarantee the rigor of our assessment, no unseen data (e.g., the unlabeled data in STL-10) was used during training.

#### 4.2. Experimental Settings

**Data Augmentation.** To ensure comparability with existing methods [4], we adopted the same data augmentation strategies, using ResNet-34 as the backbone for feature extraction. All datasets were subject to random cropping to 224x224, horizontal flipping, color jittering, and grayscale transformation. Additionally, Gaussian blur was applied to the ImageNet-10 dataset, while the upscaling of smaller datasets (CIFAR-10, CIFAR-100, and STL-10) provided a comparable blurring effect.

**Training Details.** In our experiments, both the hidden dimension and the number of features were set equal to the batch size. A cosine decay schedule without restarts [2, 23] and gradient clipping were employed to stabilize training, as validated in our ablation studies (Table 5). No additional techniques, such as self-labeling, were used to improve performance. The temperature parameters  $\tau_{\text{inst}}$  and  $\tau_{\text{feat}}$  were set to 0.5 and 1, respectively, while the balance parameter  $\alpha$  for feature diversity was set to 1. Other training settings were based on prior contrastive learning works, including 1000 training epochs, a random seed of 42, and the Adam optimizer [24] with a learning rate of  $3 \times 10^{-4}$  and no weight decay.

**Environment.** The experiments were performed on an NVIDIA RTX 3090 GPU (24GB) and an 18 vCPU AMD EPYC 9754 128-Core Processor. Batch sizes of 128 and 256 were used. Training time for CIFAR-10 and CIFAR-100 was approximately 48 GPU hours, while for STL-10 and ImageNet-10, it was around 11 GPU hours. Detailed logs of all experimental procedures are available [here](#).

**Evaluation Metrics.** We used three clustering metrics — Normalized Mutual Information (NMI), Adjusted Rand Index (ARI), and Accuracy (ACC) — to evaluate the feature extraction and disentanglement capabilities of the model.

#### 4.3. Compared Methods

We compared CD against a diverse set of representative unsupervised models, selected based on their relevance to the challenges addressed by our approach. In addition to the traditional K-means clustering algorithm [25], we assessed fully unsupervised models such as AE [7], DeCNN [26], DAE [27], VAE [8], and DCGAN [28], all of which do not rely on class information during training, like our CD model.

Furthermore, we benchmarked CD against unsupervised models that incorporate class number information, including JULE [29], DEC [30], DAC [31], DCCM [32], PICA [33], and CC [4]. All experiments were conducted using the full dataset and adhered to identical training and evaluation protocols to ensure fairness.

#### 4.4. Experimental Results

We evaluated CD at two key stages: feature extraction and feature disentanglement. K-means clustering was applied to both the backbone output and the final model output to assess performance.

**Backbone.** Table 2 presents a comparative analysis at the feature extraction stage using NMI, ARI, and ACC metrics. Across all datasets — CIFAR-10, CIFAR-100, STL-10, and ImageNet-10 — both variants of CD (CD-128 and CD-256) outperformed fully unsupervised methods such as AE, DeCNN, DAE, VAE, and DCGAN. Notably, CD

Table 2: **Feature extraction performance comparison across models.** The 1<sup>st</sup>/2<sup>nd</sup> best results are indicated in **bold**/underlined. Models that utilized class number information during training are marked with \*.

Dataset	Metrics	K-means	AE	DeCNN	DAE	VAE	DCGAN	CC*	CD-128	CD-256
CIFAR-10	NMI	0.087	0.239	0.240	0.251	0.245	0.265	0.679	<u>0.725</u>	<b>0.734</b>
	ARI	0.049	0.169	0.174	0.163	0.167	0.176	0.587	<u>0.620</u>	<b>0.635</b>
	ACC	0.229	0.314	0.282	0.297	0.291	0.315	0.752	<u>0.800</u>	<b>0.807</b>
CIFAR-100-20	NMI	0.084	0.100	0.092	0.111	0.108	0.120	0.433	<u>0.462</u>	<b>0.476</b>
	ARI	0.028	0.048	0.038	0.046	0.040	0.045	<b>0.244</b>	0.240	0.231
	ACC	0.130	0.165	0.133	0.151	0.152	0.151	<b>0.431</b>	0.418	0.422
STL-10	NMI	0.125	0.250	0.227	0.224	0.200	0.210	0.608	<u>0.670</u>	<b>0.687</b>
	ARI	0.061	0.161	0.162	0.152	0.146	0.139	0.443	<u>0.523</u>	<b>0.581</b>
	ACC	0.192	0.303	0.299	0.302	0.282	0.298	0.594	0.684	<b>0.758</b>
ImageNet-10	NMI	0.119	0.210	0.186	0.206	0.193	0.225	0.800	<b>0.893</b>	<u>0.885</u>
	ARI	0.057	0.152	0.142	0.138	0.168	0.157	0.695	<b>0.858</b>	<u>0.854</u>
	ACC	0.241	0.317	0.313	0.304	0.334	0.346	0.846	0.927	<b>0.934</b>

Table 3: **Final output performance comparison across models.** The 1<sup>st</sup>/2<sup>nd</sup> best results are indicated in **bold**/underlined. Models that utilized class number information during training are marked with \*, while those that utilized unlabeled datasets for STL-10 are marked with <sup>†</sup>.

Dataset	Metrics	JULE*	DEC* <sup>†</sup>	DAC*	DCCM*	PICA* <sup>†</sup>	CC*	CD-128	CD-256
CIFAR-10	NMI	0.192	0.257	0.396	0.496	0.591	0.705	<b>0.711</b>	<u>0.706</u>
	ARI	0.138	0.161	0.306	0.408	0.512	<b>0.637</b>	<u>0.624</u>	0.621
	ACC	0.272	0.301	0.522	0.623	0.696	<b>0.790</b>	<u>0.788</u>	0.782
CIFAR-100-20	NMI	0.103	0.136	0.185	0.285	0.310	0.417	<u>0.438</u>	<b>0.446</b>
	ARI	0.033	0.050	0.088	0.173	0.171	0.221	<u>0.249</u>	<b>0.254</b>
	ACC	0.137	0.185	0.238	0.327	0.337	<b>0.421</b>	0.394	0.416
STL-10	NMI	0.182	0.276	0.366	0.376	0.611	0.622	<b>0.687</b>	<u>0.668</u>
	ARI	0.164	0.186	0.257	0.262	0.531	0.539	<u>0.549</u>	<b>0.572</b>
	ACC	0.277	0.359	0.470	0.482	0.713	0.670	0.702	<b>0.734</b>
ImageNet-10	NMI	0.175	0.282	0.394	0.608	0.802	0.859	<b>0.898</b>	<u>0.887</u>
	ARI	0.138	0.203	0.302	0.555	0.761	0.822	<b>0.869</b>	<u>0.861</u>
	ACC	0.300	0.381	0.527	0.710	0.870	0.893	<b>0.932</b>	0.928

achieved the highest NMI scores on all datasets, with significant improvements on STL-10 and ImageNet-10, and superior overall performance compared to the class-dependent model CC.

**Final output.** Table 3 compares CD to models that use class number information. CD demonstrated strong performance across all metrics, particularly on more complex datasets like STL-10 and ImageNet-10. While ARI and ACC were slightly lower on CIFAR-10 and CIFAR-100 compared to CC, this is expected as CD does not use class number information. Importantly, CD achieved an ACC of 0.734 with a batch size of 256, surpassing PICA<sup>†</sup> (0.713) despite not using additional unlabeled data.

These results strongly support the effectiveness of CD in achieving high performance without relying on class priors. Furthermore, CD demonstrated excellent performance even with smaller batch sizes. For a t-SNE visualization of the CD-256 model’s feature representations, refer to [Appendix A](#).

#### 4.5. Ablation Studies

We conducted ablation studies on STL-10 and ImageNet-10 with a batch size of 128 to assess the contributions of different components of our model. In Sections 4.5.1 and 4.5.2, we incrementally added modules to validate their effectiveness, while in Sections 4.5.3 and 4.5.4, we removed certain modules to verify their necessity.

Table 4: Effect of normalized entropy loss (NE) and batch normalization (BN) on performance across backbone and final output.

Dataset	NE	BN	Backbone			Feature		
			NMI	ARI	ACC	NMI	ARI	ACC
STL-10	-	-	0.519 $\pm$ 0.029	0.265 $\pm$ 0.037	0.538 $\pm$ 0.050	0.352 $\pm$ 0.040	0.065 $\pm$ 0.028	0.354 $\pm$ 0.041
	✓	-	0.638 $\pm$ 0.021	0.482 $\pm$ 0.035	0.695 $\pm$ 0.031	0.656 $\pm$ 0.005	0.527 $\pm$ 0.004	0.671 $\pm$ 0.007
	-	✓	0.659 $\pm$ 0.017	0.495 $\pm$ 0.036	0.653 $\pm$ 0.037	0.367 $\pm$ 0.052	0.069 $\pm$ 0.034	0.306 $\pm$ 0.044
	✓	✓	<b>0.677 <math>\pm</math> 0.020</b>	<b>0.547 <math>\pm</math> 0.031</b>	<b>0.705 <math>\pm</math> 0.039</b>	<b>0.669 <math>\pm</math> 0.006</b>	<b>0.543 <math>\pm</math> 0.016</b>	<b>0.681 <math>\pm</math> 0.020</b>
ImageNet-10	-	-	0.632 $\pm$ 0.022	0.287 $\pm$ 0.041	0.620 $\pm$ 0.042	0.549 $\pm$ 0.038	0.163 $\pm$ 0.037	0.424 $\pm$ 0.040
	✓	-	0.748 $\pm$ 0.020	0.532 $\pm$ 0.054	0.779 $\pm$ 0.047	0.887 $\pm$ 0.002	0.861 $\pm$ 0.002	0.927 $\pm$ 0.001
	-	✓	0.837 $\pm$ 0.018	0.733 $\pm$ 0.050	0.831 $\pm$ 0.055	0.538 $\pm$ 0.043	0.152 $\pm$ 0.045	0.416 $\pm$ 0.055
	✓	✓	<b>0.857 <math>\pm</math> 0.021</b>	<b>0.772 <math>\pm</math> 0.068</b>	<b>0.858 <math>\pm</math> 0.071</b>	<b>0.890 <math>\pm</math> 0.004</b>	<b>0.864 <math>\pm</math> 0.006</b>	<b>0.929 <math>\pm</math> 0.004</b>

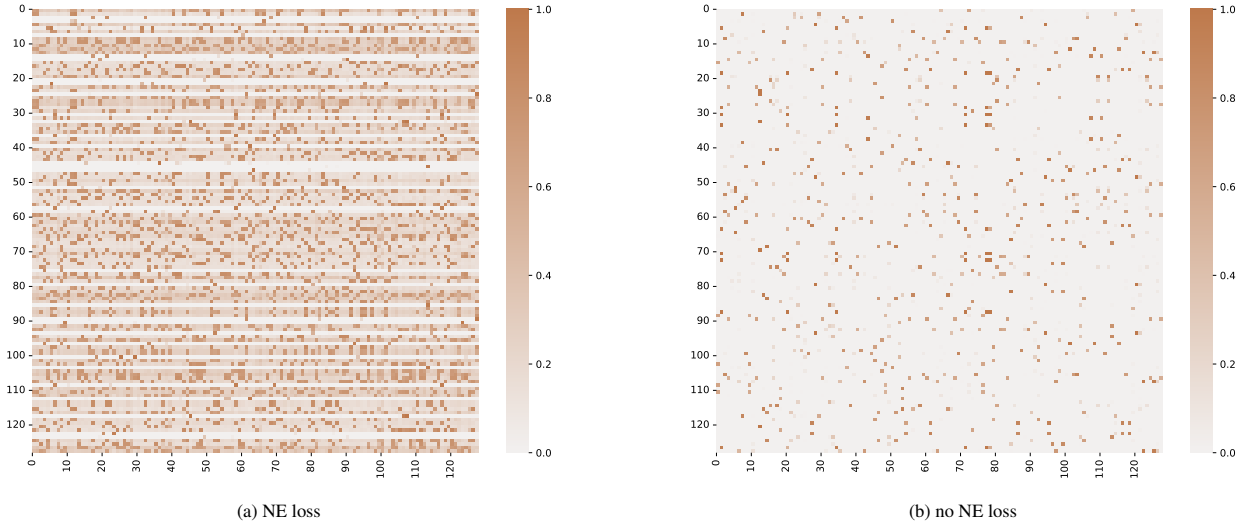


Figure 3: **Visualization of transposed model outputs with/without normalized entropy loss (NE loss).** The left figure (a) shows outputs with NE loss, emphasizing common features, while the right figure (b) shows outputs without NE loss, capturing more image-specific features.

#### 4.5.1. Normalized Entropy Loss and Batch Normalization

Table 4 demonstrates the impact of the normalized entropy loss (NE) and batch normalization (BN) on performance. Both components significantly improved results, with further enhancements observed when combined. To illustrate the effect of NE loss on feature disentanglement, Figure 3 visualizes the model’s outputs with and without NE loss. This visualization highlights the importance of NE loss in guiding the model to capture common features across the dataset.

The rows in Figure 3 represent the feature attributes learned by our model, as depicted in the feature-level part of Figure 1. Further visualization of these attributes using LIME is available in Appendix B.

#### 4.5.2. Training Tricks

Next, we evaluated the contribution of cosine decay scheduling and gradient clipping (Table 5). The results show that both techniques enhanced performance and stabilized training.

#### 4.5.3. Feature Prediction Head

We evaluated the effect of removing the feature prediction head, which reduces the model to an instance-level contrastive learning framework similar to SimCLR. As shown in Table 6, the feature prediction head significantly boosts performance, and its removal results in substantial degradation, highlighting the critical role of feature-level contrastive learning in effective disentanglement (see Table C.9 for backbone results).

Table 5: Effect of cosine decay schedule (Sch.) and gradient clipping (Clip.) on model performance.

Dataset	Sch. & Clip.	NMI	ARI	ACC
STL-10	-	$0.669 \pm 0.006$	$0.543 \pm 0.016$	$0.681 \pm 0.020$
	✓	<b><math>0.679 \pm 0.007</math></b>	<b><math>0.564 \pm 0.023</math></b>	<b><math>0.720 \pm 0.026</math></b>
ImageNet-10	-	$0.890 \pm 0.004$	$0.864 \pm 0.006$	$0.929 \pm 0.004$
	✓	<b><math>0.898 \pm 0.003</math></b>	<b><math>0.868 \pm 0.006</math></b>	<b><math>0.931 \pm 0.003</math></b>

Table 6: Effect of feature-level head on model performance.

Dataset	Feature-Level Head	NMI	ARI	ACC
STL-10	-	$0.599 \pm 0.029$	$0.458 \pm 0.043$	$0.649 \pm 0.053$
	✓	<b><math>0.679 \pm 0.007</math></b>	<b><math>0.564 \pm 0.023</math></b>	<b><math>0.720 \pm 0.026</math></b>
ImageNet-10	-	$0.708 \pm 0.031$	$0.413 \pm 0.060$	$0.608 \pm 0.065$
	✓	<b><math>0.898 \pm 0.003</math></b>	<b><math>0.868 \pm 0.006</math></b>	<b><math>0.931 \pm 0.003</math></b>

In comparison to SimCLR under identical training settings, our model demonstrates significant improvements: on the STL-10 dataset, NMI increases by 13.4%, ARI by 23.1%, and ACC by 10.9%; on ImageNet-10, NMI improves by 26.8%, ARI by 110.2%, and ACC by 53.1%. These results present that our feature-level contrastive learning approach enables the model to capture more distinct and diverse semantic features, leading to improved clustering and representation quality in the final output.

#### 4.5.4. Data Augmentation

Finally, we examined the necessity of the dual-view data augmentation strategy (Table 7). The results indicate that dual-view augmentation is critical for feature disentanglement, whereas single-view augmentation can still achieve satisfactory performance during feature extraction (see Table C.10 for details).

Table 7: Effect of single-view vs. dual-view data augmentation on model performance.

Dataset	$x^{(1)}$	$x^{(2)}$	NMI	ARI	ACC
STL-10	-	✓	$0.643 \pm 0.004$	$0.555 \pm 0.012$	$0.717 \pm 0.014$
	✓	✓	<b><math>0.679 \pm 0.008</math></b>	<b><math>0.564 \pm 0.023</math></b>	<b><math>0.720 \pm 0.026</math></b>
ImageNet-10	-	✓	$0.874 \pm 0.001$	$0.847 \pm 0.001$	$0.918 \pm 0.001$
	✓	✓	<b><math>0.898 \pm 0.003</math></b>	<b><math>0.868 \pm 0.006</math></b>	<b><math>0.931 \pm 0.003</math></b>

## 5. Conclusion

In this work, we propose a novel framework that eliminates the reliance on class number assumptions, enabling the model to operate without predefined task constraints. By integrating multi-level contrastive learning with a disentanglement loss, our framework captures more fine-grained features from the data. Our experiments reveal that CD achieves comparable performance to class-dependent methods on smaller datasets (CIFAR-10, CIFAR-100), and outperforms them on more complex datasets (STL-10, ImageNet-10), despite its simple architecture. Ablation studies further confirm the effectiveness of each component. Moreover, our framework ensures that the final model outputs are enriched with semantic information, enhancing the interpretability of the learned features.

## 6. Acknowledgments

This paper was supported by the Fujian Provincial Natural Science Foundation of China (No.2021J01129), the Fujian Provincial Higher Education Technology Research Association Fund Project (No.H2000134A), and the Fujian

Agriculture and Forestry University Horizontal Technology Innovation Fund (No.KHF190015).

### Appendix A. t-SNE Visualization of Backbone and Feature Predictor Outputs

In this appendix, we present the t-SNE (t-Distributed Stochastic Neighbor Embedding) visualizations [34] of the outputs both the backbone feature extraction layer and the feature predictor of our model, across all datasets: CIFAR-10, CIFAR-100, STL-10, and ImageNet-10. These visualizations are shown in Figures A.4-A.7, where (a) represents the backbone output and (b) represents the feature predictor output for each dataset.

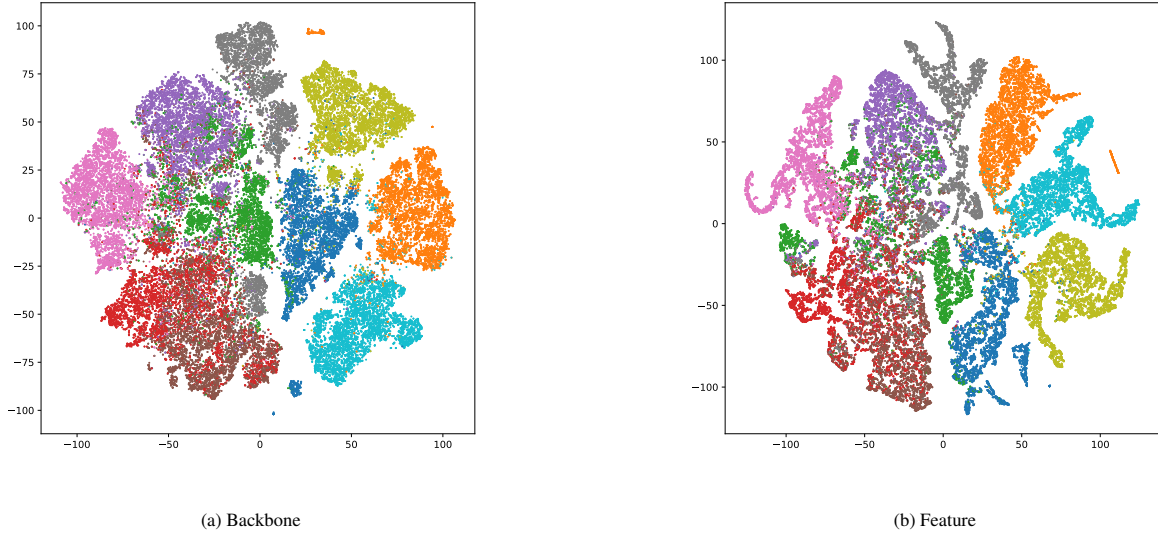


Figure A.4: t-SNE visualization for CIFAR-10

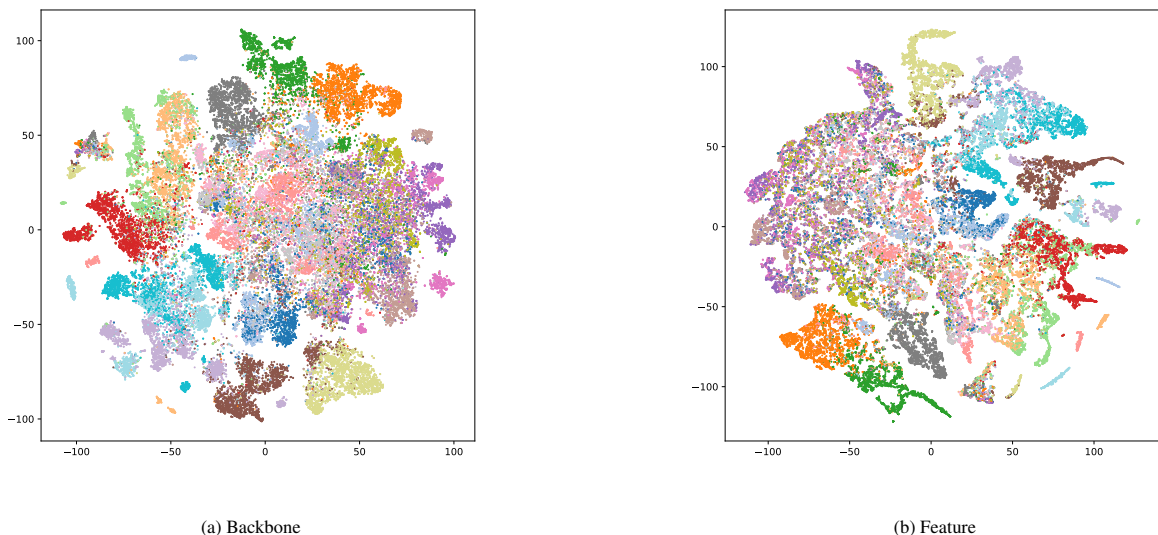


Figure A.5: t-SNE visualization for CIFAR-100

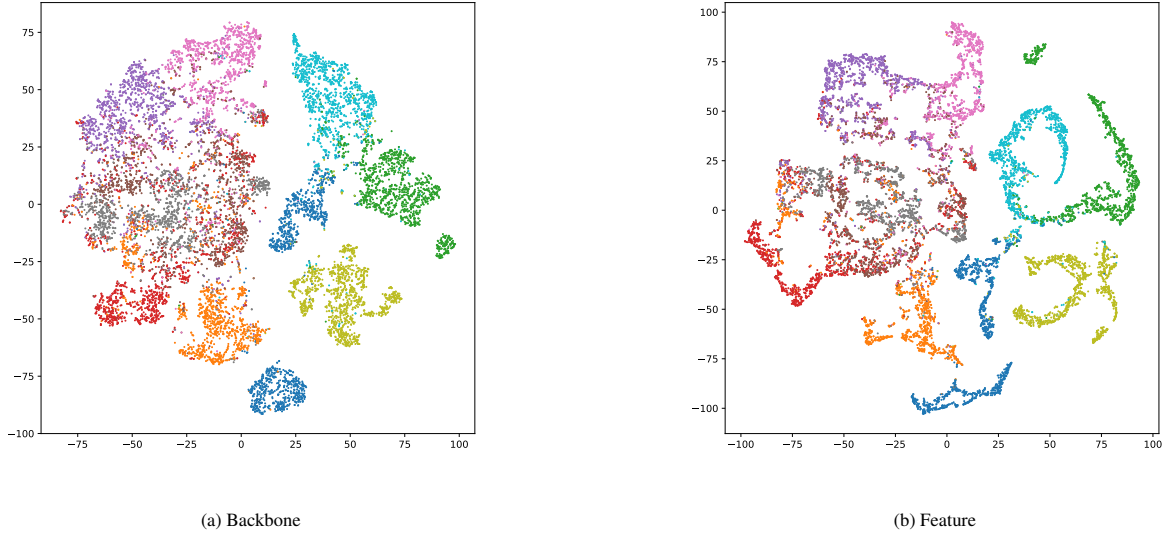


Figure A.6: t-SNE visualization for STL-10

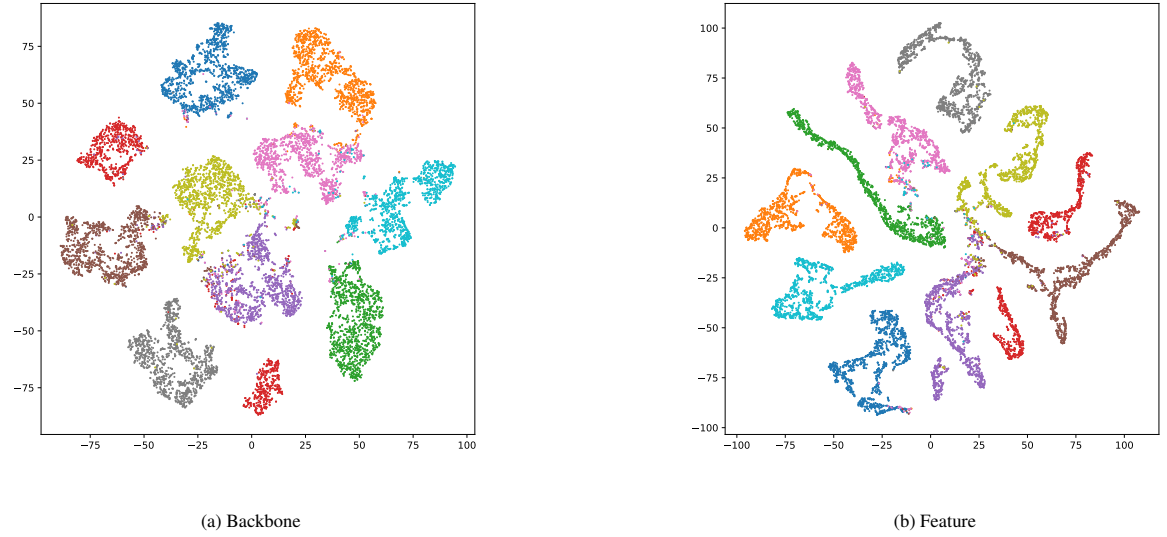


Figure A.7: t-SNE visualization for ImageNet-10

## Appendix B. Visualizing Feature Prediction Heads with LIME

We utilize the **LIME** (Local Interpretable Model-Agnostic Explanations) technique [6] to visualize the outputs of the feature prediction heads. LIME is configured with *num\_samples*=5000, meaning that for each image, LIME generates 5000 perturbed samples to create an interpretable explanation. We only visualize images where the feature prediction heads produce outputs greater than **0.75**.

The feature prediction heads visualized in Figure B.8 correspond to the indices 1, 5, 6, 17, and 18. These specific heads were selected to ensure a visually meaningful comparison, as some other heads produced fewer than six images

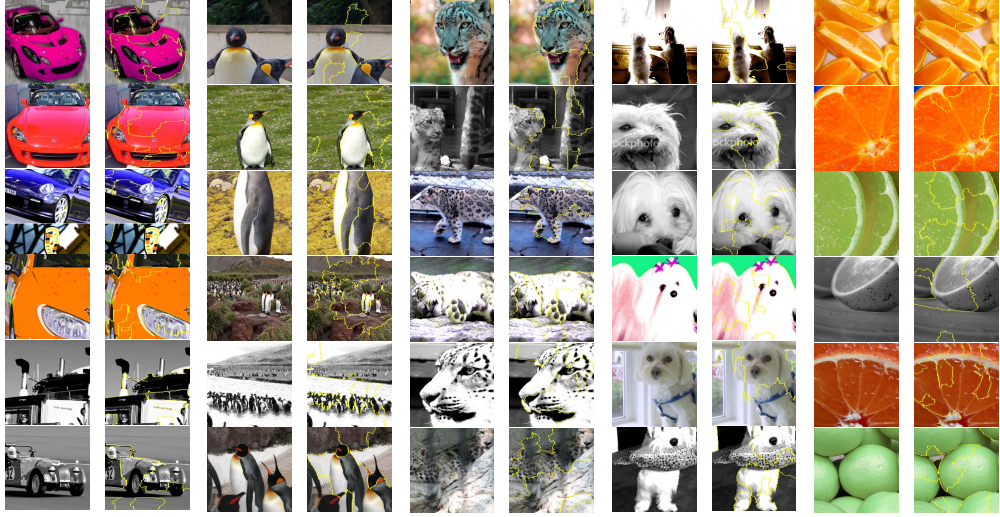


Figure B.8: Visualization of the attention from five feature prediction heads, with yellow-circled areas highlighting the regions that the heads focus on.

that met the 0.75 threshold. The yellow highlighted areas indicate the regions that these heads attend to.

Figure B.9 presents the same heads applied to a new batch of images, with a mask applied to remove areas that were not attended to.

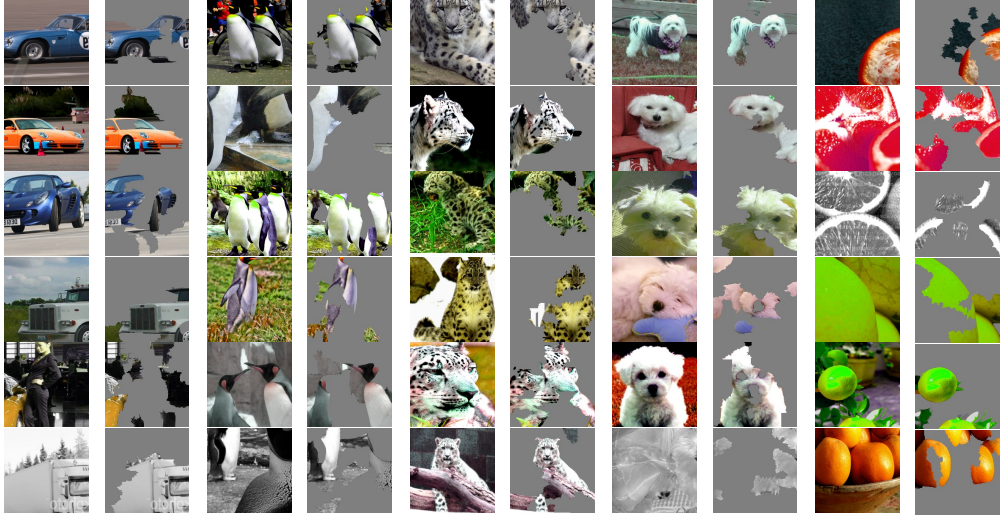


Figure B.9: Visualization of the same five feature prediction heads on a new batch of images, with non-attended regions masked out.

The model used for this visualization was pre-trained on the **ImageNet-10** dataset with the following hyperparameters: batch size=256, epochs=1000, and learning rate=0.0003. All other settings were kept as defaults from our [repository](#), where the pre-trained model files and complete experimental processes for all other experiments in this study are also available.

### Appendix C. Ablation Studies on Backbone Feature Extraction

This section provides additional ablation studies focused on evaluating the backbone feature extraction capabilities of our proposed framework. These experiments assess the contribution of various framework components by examin-

ing their impact on the backbone’s ability to extract meaningful features. Specifically, we analyze the performance of the backbone under different configurations by removing or modifying key components such as the instance projector, feature predictor, and data augmentation strategies.

The experiments are conducted on the STL-10 and ImageNet-10 datasets with the same batch size of 128, as used in the main experiments. We report the results using metrics such as Normalized Mutual Information (NMI), Adjusted Rand Index (ARI), and Accuracy (ACC). The backbone performance is compared across several configurations to highlight the individual and combined impact of the modules on feature extraction.

Table C.8: Effect of cosine decay schedule (Sch.) and gradient clipping (Clip.) on feature extraction.

Dataset	Scheduler & Grad Clipping	Backbone		
		NMI	ARI	ACC
STL-10	-	<b>0.677 ± 0.020</b>	<b>0.547 ± 0.031</b>	<b>0.705 ± 0.039</b>
	✓	0.674 ± 0.015	0.545 ± 0.032	0.701 ± 0.034
ImageNet-10	-	0.857 ± 0.021	0.772 ± 0.068	0.858 ± 0.071
	✓	<b>0.886 ± 0.008</b>	<b>0.844 ± 0.022</b>	<b>0.918 ± 0.026</b>

Table C.9: Effect of feature-level head on feature extraction.

Dataset	Feature-Level	Backbone		
		NMI	ARI	ACC
STL-10	-	0.659 ± 0.016	0.530 ± 0.028	0.692 ± 0.030
	✓	<b>0.674 ± 0.015</b>	<b>0.545 ± 0.032</b>	<b>0.701 ± 0.034</b>
ImageNet-10	-	0.870 ± 0.022	0.809 ± 0.064	0.886 ± 0.058
	✓	<b>0.886 ± 0.008</b>	<b>0.844 ± 0.022</b>	<b>0.918 ± 0.026</b>

Table C.10: Effect of single-view vs. dual-view data augmentation on feature extraction.

Dataset	Augmentation	Backbone			
		x1	x2	NMI	ARI
STL-10	-	✓	0.660 ± 0.011	0.520 ± 0.022	0.683 ± 0.022
	✓	✓	<b>0.671 ± 0.019</b>	<b>0.545 ± 0.032</b>	<b>0.701 ± 0.034</b>
ImageNet-10	-	✓	<b>0.889 ± 0.010</b>	<b>0.851 ± 0.024</b>	<b>0.923 ± 0.018</b>
	✓	✓	0.886 ± 0.008	0.844 ± 0.022	0.918 ± 0.026

It can be observed that when evaluating the model’s ability as a pretext model, or more specifically, the feature extraction capability of the backbone, the scheduler, gradient clipping, and dual-view data augmentation are not essential. However, if we aim for the final output of the model to be meaningful, rather than focusing solely on intermediate states, these components become crucial. You may refer to Table 5 - Table 7, especially Table 6, where our model demonstrates significantly higher semantic expressiveness in the final layer.

## References

- [1] M. Ye, X. Zhang, P. C. Yuen, S.-F. Chang, Unsupervised embedding learning via invariant and spreading instance feature, in: Proceedings of the IEEE/CVF conference on computer vision and pattern recognition, 2019, pp. 6210–6219.
- [2] T. Chen, S. Kornblith, M. Norouzi, G. Hinton, A simple framework for contrastive learning of visual representations, in: International conference on machine learning, PMLR, 2020, pp. 1597–1607.

- [3] W. Van Gansbeke, S. Vandenhende, S. Georgoulis, M. Proesmans, L. Van Gool, Scan: Learning to classify images without labels, in: European conference on computer vision, Springer, 2020, pp. 268–285.
- [4] Y. Li, P. Hu, Z. Liu, D. Peng, J. T. Zhou, X. Peng, Contrastive clustering, in: Proceedings of the AAAI conference on artificial intelligence, volume 35, 2021, pp. 8547–8555.
- [5] Q. Qian, Stable cluster discrimination for deep clustering, in: Proceedings of the IEEE/CVF International Conference on Computer Vision, 2023, pp. 16645–16654.
- [6] M. T. Ribeiro, S. Singh, C. Guestrin, " why should i trust you?" explaining the predictions of any classifier, in: Proceedings of the 22nd ACM SIGKDD international conference on knowledge discovery and data mining, 2016, pp. 1135–1144.
- [7] Y. Bengio, P. Lamblin, D. Popovici, H. Larochelle, Greedy layer-wise training of deep networks, Advances in neural information processing systems 19 (2006).
- [8] D. Kingma, Auto-encoding variational bayes, arXiv preprint arXiv:1312.6114 (2013).
- [9] I. Goodfellow, J. Pouget-Abadie, M. Mirza, B. Xu, D. Warde-Farley, S. Ozair, A. Courville, Y. Bengio, Generative adversarial nets, Advances in neural information processing systems 27 (2014).
- [10] F. Ntelemis, Y. Jin, S. A. Thomas, A generic self-supervised framework of learning invariant discriminative features, IEEE Transactions on Neural Networks and Learning Systems (2023).
- [11] K. He, H. Fan, Y. Wu, S. Xie, R. Girshick, Momentum contrast for unsupervised visual representation learning, in: Proceedings of the IEEE/CVF conference on computer vision and pattern recognition, 2020, pp. 9729–9738.
- [12] J.-B. Grill, F. Strub, F. Altché, C. Tallec, P. Richemond, E. Buchatskaya, C. Doersch, B. Avila Pires, Z. Guo, M. Gheshlaghi Azar, et al., Bootstrap your own latent-a new approach to self-supervised learning, Advances in neural information processing systems 33 (2020) 21271–21284.
- [13] X. Chen, K. He, Exploring simple siamese representation learning, in: Proceedings of the IEEE/CVF conference on computer vision and pattern recognition, 2021, pp. 15750–15758.
- [14] C. Niu, H. Shan, G. Wang, Spice: Semantic pseudo-labeling for image clustering, IEEE Transactions on Image Processing 31 (2022) 7264–7278.
- [15] K. He, X. Zhang, S. Ren, J. Sun, Deep residual learning for image recognition, in: Proceedings of the IEEE conference on computer vision and pattern recognition, 2016, pp. 770–778.
- [16] S. Ioffe, Batch normalization: Accelerating deep network training by reducing internal covariate shift, arXiv preprint arXiv:1502.03167 (2015).
- [17] K. Sohn, Improved deep metric learning with multi-class n-pair loss objective, Advances in neural information processing systems 29 (2016).
- [18] Z. Wu, Y. Xiong, S. X. Yu, D. Lin, Unsupervised feature learning via non-parametric instance discrimination, in: Proceedings of the IEEE conference on computer vision and pattern recognition, 2018, pp. 3733–3742.
- [19] A. v. d. Oord, Y. Li, O. Vinyals, Representation learning with contrastive predictive coding, arXiv preprint arXiv:1807.03748 (2018).
- [20] A. Krizhevsky, G. Hinton, Learning multiple layers of features from tiny images, Technical report, University of Toronto, 2009. URL: <https://www.cs.toronto.edu/~kriz/learning-features-2009-TR.pdf>.
- [21] A. Coates, A. Ng, H. Lee, An analysis of single-layer networks in unsupervised feature learning, in: Proceedings of the fourteenth international conference on artificial intelligence and statistics, JMLR Workshop and Conference Proceedings, 2011, pp. 215–223.
- [22] J. Deng, W. Dong, R. Socher, L.-J. Li, K. Li, L. Fei-Fei, Imagenet: A large-scale hierarchical image database, in: 2009 IEEE conference on computer vision and pattern recognition, Ieee, 2009, pp. 248–255.
- [23] I. Loshchilov, F. Hutter, Sgdr: Stochastic gradient descent with warm restarts, arXiv preprint arXiv:1608.03983 (2016).
- [24] D. P. Kingma, Adam: A method for stochastic optimization, arXiv preprint arXiv:1412.6980 (2014).
- [25] J. MacQueen, et al., Some methods for classification and analysis of multivariate observations, in: Proceedings of the fifth Berkeley symposium on mathematical statistics and probability, volume 1, Oakland, CA, USA, 1967, pp. 281–297.
- [26] M. D. Zeiler, D. Krishnan, G. W. Taylor, R. Fergus, Deconvolutional networks, in: 2010 IEEE Computer Society Conference on computer vision and pattern recognition, IEEE, 2010, pp. 2528–2535.
- [27] P. Vincent, H. Larochelle, I. Lajoie, Y. Bengio, P.-A. Manzagol, L. Bottou, Stacked denoising autoencoders: Learning useful representations in a deep network with a local denoising criterion., Journal of machine learning research 11 (2010).
- [28] A. Radford, Unsupervised representation learning with deep convolutional generative adversarial networks, arXiv preprint arXiv:1511.06434 (2015).
- [29] J. Yang, D. Parikh, D. Batra, Joint unsupervised learning of deep representations and image clusters, in: Proceedings of the IEEE conference on computer vision and pattern recognition, 2016, pp. 5147–5156.
- [30] J. Xie, R. Girshick, A. Farhadi, Unsupervised deep embedding for clustering analysis, in: International conference on machine learning, PMLR, 2016, pp. 478–487.
- [31] J. Chang, L. Wang, G. Meng, S. Xiang, C. Pan, Deep adaptive image clustering, in: Proceedings of the IEEE international conference on computer vision, 2017, pp. 5879–5887.
- [32] J. Wu, K. Long, F. Wang, C. Qian, C. Li, Z. Lin, H. Zha, Deep comprehensive correlation mining for image clustering, in: Proceedings of the IEEE/CVF international conference on computer vision, 2019, pp. 8150–8159.
- [33] J. Huang, S. Gong, X. Zhu, Deep semantic clustering by partition confidence maximisation, in: Proceedings of the IEEE/CVF conference on computer vision and pattern recognition, 2020, pp. 8849–8858.
- [34] L. Van der Maaten, G. Hinton, Visualizing data using t-sne., Journal of machine learning research 9 (2008).